



Characterization of the Secondary Neutron Field Produced in a Thick Aluminum Shield by 1 GeV/u ⁵⁶Fe Ions Using TLD-Based Ambient Dosimeters

Daria Boscolo¹, Daniela Scognamiglio^{1,2}, Felix Horst^{1,3*}, Uli Weber¹, Christoph Schuy¹, Marco Durante^{1,4}, Chiara La Tessa⁵, Ekaterina Kozlova¹, Alexey Sokolov¹, Irina Dinescu⁶, Torsten Radon¹, Désirée Radeck⁷ and Miroslav Zbořil⁷

¹ Biophysics Department, GSI Helmholtzzentrum für Schwerionenforschung GmbH, Darmstadt, Germany, ² Department of Physics, University of Naples Federico II, Naples, Italy, ³ Institute of Medical Physics and Radiation Protection, Technische Hochschule Mittelhessen, Giessen, Germany, ⁴ Institute of Solid State Physics, Technical University Darmstadt, Darmstadt, Germany, ⁵ University of Trento and Trento Institute for Fundamental Physics and Applications (TIFPA), Istituto nazionale di fisica nucleare (INFN), Povo, Italy, ⁶ Horia Hulubei National Institute for Research and Development in Physics and Nuclear Engineering and Faculty of Applied Physics, University Politehnica of Bucharest, Bucharest, Romania, ⁷ Physikalisch-Technische Bundesanstalt, Braunschweig, Germany

OPEN ACCESS

Edited by:

Paul Sellin,
University of Surrey, United Kingdom

Reviewed by:

Hector Rene Vega-Carrillo,
Autonomous University of
Zacatecas, Mexico
Zhonglu Wang,
Penn State Milton S. Hershey Medical
Center, United States

*Correspondence:

Felix Horst
f.horst@gsi.de

Specialty section:

This article was submitted to
Radiation Detectors and Imaging,
a section of the journal
Frontiers in Physics

Received: 22 June 2020

Accepted: 28 July 2020

Published: 29 October 2020

Citation:

Boscolo D, Scognamiglio D, Horst F, Weber U, Schuy C, Durante M, La Tessa C, Kozlova E, Sokolov A, Dinescu I, Radon T, Radeck D and Zbořil M (2020) Characterization of the Secondary Neutron Field Produced in a Thick Aluminum Shield by 1 GeV/u ⁵⁶Fe Ions Using TLD-Based Ambient Dosimeters. *Front. Phys.* 8:365. doi: 10.3389/fphy.2020.00365

The neutron ambient dose equivalent induced by galactic cosmic-ray-like (1 GeV/u ⁵⁶Fe) radiation stopped in a thick aluminum shield was measured at different angles with a GSI neutron ball, the standard TLD (thermoluminescent dosimeters)-based neutron dosimeter for area monitoring at the GSI facility. In order to measure reliably at large angles, a modified version of the GSI ball, including a set of three more sensitive TLD600H/700H cards, instead of one standard TLD600/700 card was used. The modified GSI balls were calibrated in neutron reference fields of ²⁴¹Am-Be(α ,n) available at the Physikalisch-Technische Bundesanstalt (PTB). The neutron ambient dose equivalent was measured at five different angles (15, 40, 90, 115, and 130 degrees) with respect to the beam direction and compared to the calculated detector response and neutron ambient dose equivalent results from FLUKA simulations. The dosimeter readings were corrected for signal contributions coming from secondary charged particles. An agreement within 15% was found between the measured and calculated GSI ball response and an agreement within 30% was found between experiments and calculated neutron dose equivalents.

Keywords: space radiation shielding, neutron production, ion fragmentation, TLD, neutron detectors, Monte Carlo

1. INTRODUCTION

Long-term manned space missions to Mars and the construction of a permanent Moon base with a large crew both represent two of the most challenging new frontiers of human space flight exploration. However, the effects of space radiation on the health of astronauts is one of the most serious limiting factors to the realization of such explorations [1–3]. In order to predict the biological effects of radiation exposure and develop possible mitigation strategies, space agencies are developing complex risk models [4, 5]. However, the predictability of these models is strongly

limited by the large uncertainties of the basic physical and radiobiological models and the limited amount of experimental data for the reaction and production cross-sections of particles from galactical cosmic radiation (GCR) [6].

When studying shielding approaches for planetary habitats, the exploitation of *in-situ* materials to build very thick shielding represents one of the most realistic strategies with which to maximize shielding efficiency while limiting costs. In this context, the lack of experimental data on neutron and light ion production after thick shielding material by highly energetic ion radiation represents one of these significant knowledge gaps. Recent studies demonstrated that, behind thick shielding ($\geq 20 \text{ g/cm}^2$), up to 80–90% of the total dose equivalent to various body organs comes from light secondary fragments and neutrons [7–9]. In particular, secondary neutrons—abundantly produced through all phases of a nuclear fragmentation process—represent a severe threat for the astronauts' health due to their high penetration length and their increased biological effectiveness.

Motivated by these gaps in data, a series of experimental studies for secondary particle production in thick targets for space radiation protection applications have been performed at the HIMAC accelerator in Japan by NASA-associated research groups from the USA; more recent studies have been performed at NSRL at Brookhaven National Laboratory [10–12]. However, despite the significant experimental effort invested in these campaigns, measurement gaps are still reported [13].

Radiation transport codes represent a powerful and very important tool for radiation protection in space. However, the uncertainties regarding the nuclear physics models and the lack of necessary experimental data needed to improve these models lead to large differences among the major particle transport codes used for space radiation application [14]. Recent studies demonstrated that different Monte Carlo (MC) codes could reproduce the measured neutron dose distributions behind shielding materials irradiated with protons only with an accuracy of a factor of two [15].

In this context, an accelerator-based experimental campaign within the framework of the ESA-IBER program is currently taking place in Cave A of GSI (Helmholtzzentrum für Schwerionenforschung, Darmstadt) by a collaboration with the PTB (Physikalisch-Technische Bundesanstalt, Braunschweig), TIFPA (Trento Institute of Fundamental Physics and Application, Trento), the Radiation protection department of GSI, and the Biophysics department of GSI. This project aims at a full characterization of the neutron and light fragment field generated by galactic cosmic ray-like radiation (1 GeV/u ^{56}Fe ions) fully stopping in a thick aluminum target. The measurement method consists of a multi-detector system including four complementary detectors and measurement techniques. In particular, the secondary neutron yield and the neutron ambient dose equivalent at different angles will be measured with the active PTB Bonner sphere spectrometer (BSS) NEMUS and the TLD-based GSI neutron ball dosimeters, respectively. The double differential yield of the secondary fragments will be measured with ToF (Time of flight) and energy loss measurements via ΔE -E telescopes while the TEPC (tissue equivalent proportional counter) will

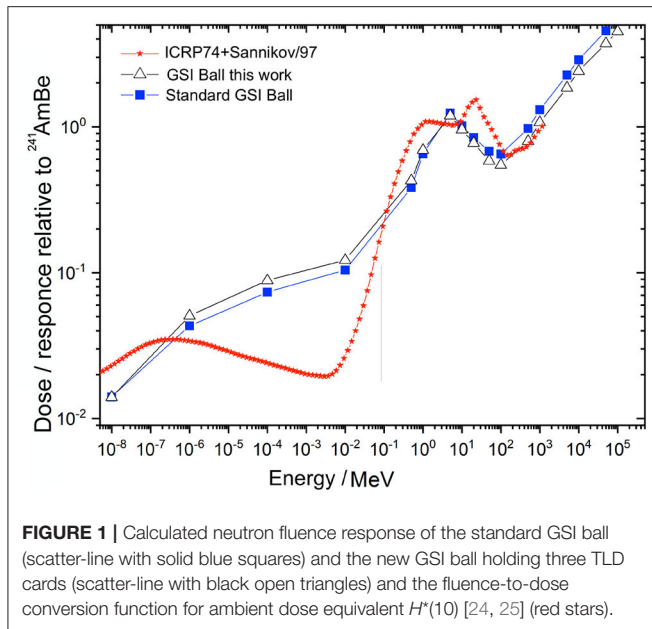
allow a microdosimetric characterization in terms of lineal energy spectra.

In this work, the results obtained from GSI neutron balls within the first experimental run are presented. These dosimeters, consisting of a moderator sphere equipped with thermoluminescence dosimeters (TLDs) sensitive to thermal neutrons, have been used to measure the angular distribution of the neutron ambient dose equivalent around a thick target at different angular positions. For this experimental campaign, a modified version of the GSI ball, including a set of three sensitive TLD600H/700H cards, was used. In order to achieve the maximum accuracy, the full detector setup was calibrated in the PTB $^{241}\text{Am-Be}(\alpha, n)$ neutron reference field. After describing the calibration procedure, and the experimental setup, the measured neutron ambient dose equivalent distribution is presented. A dedicated study is carried out to quantify the signal contributions coming from secondary protons interacting with the GSI balls. Consequently, the dosimeter readings are corrected for this over-response due to secondary protons. The experimental results are finally compared with Monte Carlo simulations showing a good agreement between the measured and calculated neutron dose equivalent distribution.

2. MATERIALS AND METHODS

2.1. GSI Ball: A TLD-Based Neutron Dosimeter

GSI balls are the standard neutron dosimeters used at the GSI (Helmholtzzentrum für Schwerionenforschung in Darmstadt) accelerator site for environmental monitoring all over the facility [16–18]. The detectors consist of a 32 cm diameter polyethylene sphere (density 0.954 g/cm^3) with a 1 cm thick lead layer inside. At the sphere center, a TLD card of the Harshaw type is used as the radiation-sensitive element. The polyethylene moderates up to 10 MeV neutrons down to thermal energies so that they can be detected by the TLDs. For more energetic neutrons, for which the polyethylene moderator becomes insufficient, a lead layer converts the high-energy neutrons into detectable evaporation neutrons by spallation reactions. The geometrical design of the GSI ball dosimeter was optimized through Monte Carlo transport codes (FLUKA and MCNPX) [19, 20] to reproduce the ambient dose equivalent, $H^*(10)$, (as given in the ICRP74 [21]) in a neutron energy range spanning from thermal up to GeVs. The calculated response was validated with mono-energetic neutron beams up to 19 MeV and quasi-mono-energetic neutrons of 500 and 800 MeV [22, 23]. In **Figure 1**, the response function of the new GSI ball dosimeters is depicted together with the response function of the standard model of GSI ball (with one card) and with the energy-dependent dose equivalent curve from [24, 25]. Within this project, five GSI balls were used to measure the neutron-ambient dose equivalent at different angles; among these, three were a new prototype able to hold up to three TLD cards, thus providing improved measurement statistics. A schematic representation of a GSI ball from a different projection and of the sensitive element consisting of a



cylindrical insert holding the three TLD600H/TLD700H cards is shown in **Figure 2**.

The TLD cards contain two pairs of different TLD chips based on LiF: two TLD600 and two TLD700. The two TLD600 chips, enriched in ^6Li , can detect photons, charged particles and thermal neutrons (through the $^6\text{Li}(n,\alpha)^3\text{H}$ reaction), while the two TLD700 chips, where the ^6Li fraction has been depleted, respond identically to the TLD600 to gamma radiation and charged particles but are not as sensitive to thermal neutrons. This allows a separation of the neutron TL signal in a mixed radiation field by subtraction of the TLD700 signal from the one measured by the TLD600 [26–28]. The readout procedure of the TLD600H/700H crystals is described in the **Supplementary Material**. In this work, to measure accurately at positions where the neutron yield is very low (large angles and backwards positions), the standard TLD600/700 cards were replaced by more sensitive TLD600H/700H cards [29], which are able to provide reliable readings from doses of two μGy instead of 20 μGy [30]. The higher sensitivity (TL light output per absorbed dose) is achieved by different doping of the LiF material (doped with Mg, Cu and P instead of Mg and Ti). However, the different composition does not only affect the sensitivity but also the dose-response function and saturation behavior and consequently also the relative TL efficiency for densely ionizing radiation. Even though the TLD600H/700H material is expected to be 10–30 times more sensitive to photons than the standard TLD600/700 chips [31], for neutron dosimetry, this higher sensitivity is reduced (for the chips used in this work) to only a factor of 7 when considering also the difference of the relative TL efficiency to thermal neutrons. This quantity is about a factor of 3 lower for the TLD600H material compared to TLD600. This can be explained by the higher sensitivity at low doses since to the Mg, Cu, and P doping goes along with a lower saturation level. The factor of

3 observed in this work is in accordance with the prediction by microscopic models [32].

2.1.1. Dosimeter Calibration

All TLD600H/700H cards used during this project have been calibrated, in terms of dose per TL signal, with gamma radiation from a ^{137}Cs source available at GSI with a nominal activity of 364 MBq. Response factors to gamma radiation, R_γ , obtained for all crystals (four per card) are shown separately for TLD600H and TLD700H in the **Supplementary Material**. Averaging all irradiated crystals, it can be observed that both TLD types show the same R_γ : an average response of $0.59 \text{ nC } \mu\text{Gy}^{-1}$ (with a maximum of $0.69 \text{ nC } \mu\text{Gy}^{-1}$ and a minimum of $0.45 \text{ nC } \mu\text{Gy}^{-1}$) for TLD600H and $0.57 \text{ nC } \mu\text{Gy}^{-1}$ (with a maximum of $0.66 \text{ nC } \mu\text{Gy}^{-1}$ and a minimum of $0.49 \text{ nC } \mu\text{Gy}^{-1}$) for TLD700H. A large response variability between the crystals is observed and has to be taken into account when performing precision measurements, thus exhibiting the need for individual crystal calibration.

After determining the response of every single crystal to gamma radiation, all the GSI balls used during the experiments were calibrated in terms of the neutron ambient dose equivalent using the neutron field generated by a $^{241}\text{Am-Be}(\alpha,n)$ source available at GSI with a nominal activity of 370 GBq. A detailed description of the neutron calibration procedure performed can be found in [20]. To exclude any uncertainties coming from the dosimeter setup, the calibration was performed with the exact same combination of cards and moderators used during the experiment. An additional calibration for a single GSI ball holding three cards was performed with the reference $^{241}\text{Am-Be}(\alpha,n)$ source at PTB. On this occasion, corrections for the scattered neutrons contributions have been made by means of the shadow cones technique [33, 34]. A difference of 20% was found between the average neutron response, R_n , measured at GSI and the ones measured at PTB, probably coming from the missing correction for the scattered neutron contribution at GSI. Neutron calibration results with the $^{241}\text{Am-Be}(\alpha,n)$ are reported in the **Supplementary Material**.

2.2. Experimental Setup

Two sets of five neutron dosimeters were irradiated in the secondary radiation field generated by the nuclear interaction of a 1 GeV/u ^{56}Fe beam fully stopped in a cylindrical aluminum target 20 cm in diameter with a height of 20 cm in GSI's Cave A. The primary radiation and the target selection was chosen to be relevant for space shielding applications: the 1 GeV/u ^{56}Fe beam is often used as reference radiation for studying GCR, and aluminum constitutes one of the main construction material for spacecrafts and is typically used as reference material. The neutron ambient dose equivalent was measured at 5 different angles with respect to the beam axis at (15, 40, 90, 115, and 130 degrees). Two independent repetitions of the experiment have been performed in order to guarantee the measurement reproducibility. Each measurement set was composed by three new GSI ball prototypes (holding three TLD600H/TLD700H cards) and two standard GSI ball dosimeter (holding one TLD card) respectively at angles of 15, 40, and 130 degrees and at 90 and 115 degrees. A schematic representation of the experimental

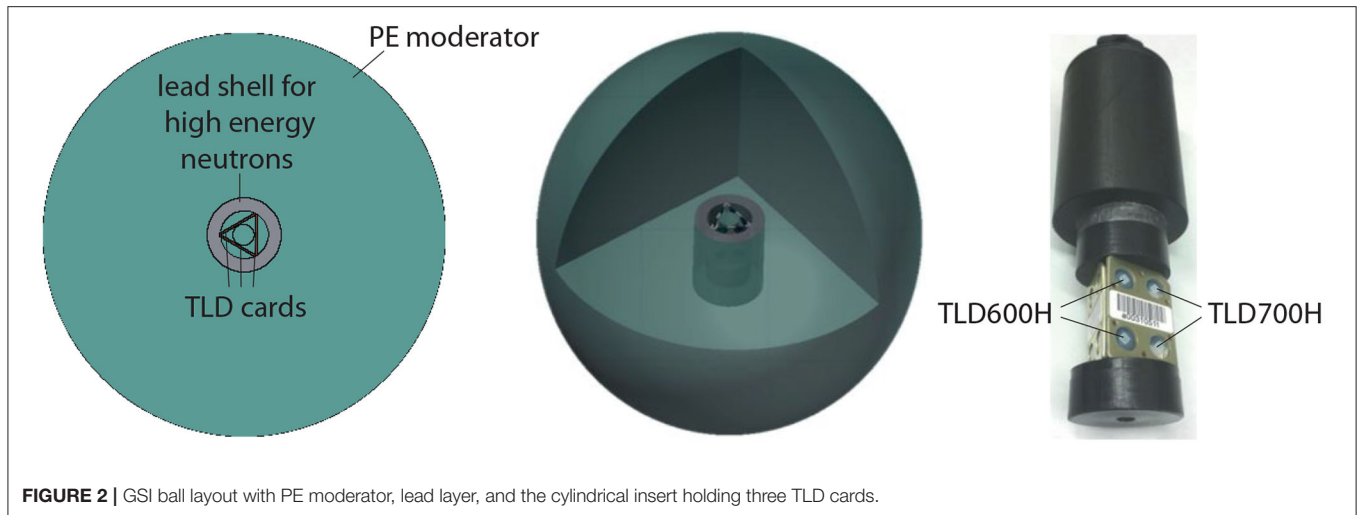


FIGURE 2 | GSI ball layout with PE moderator, lead layer, and the cylindrical insert holding three TLD cards.

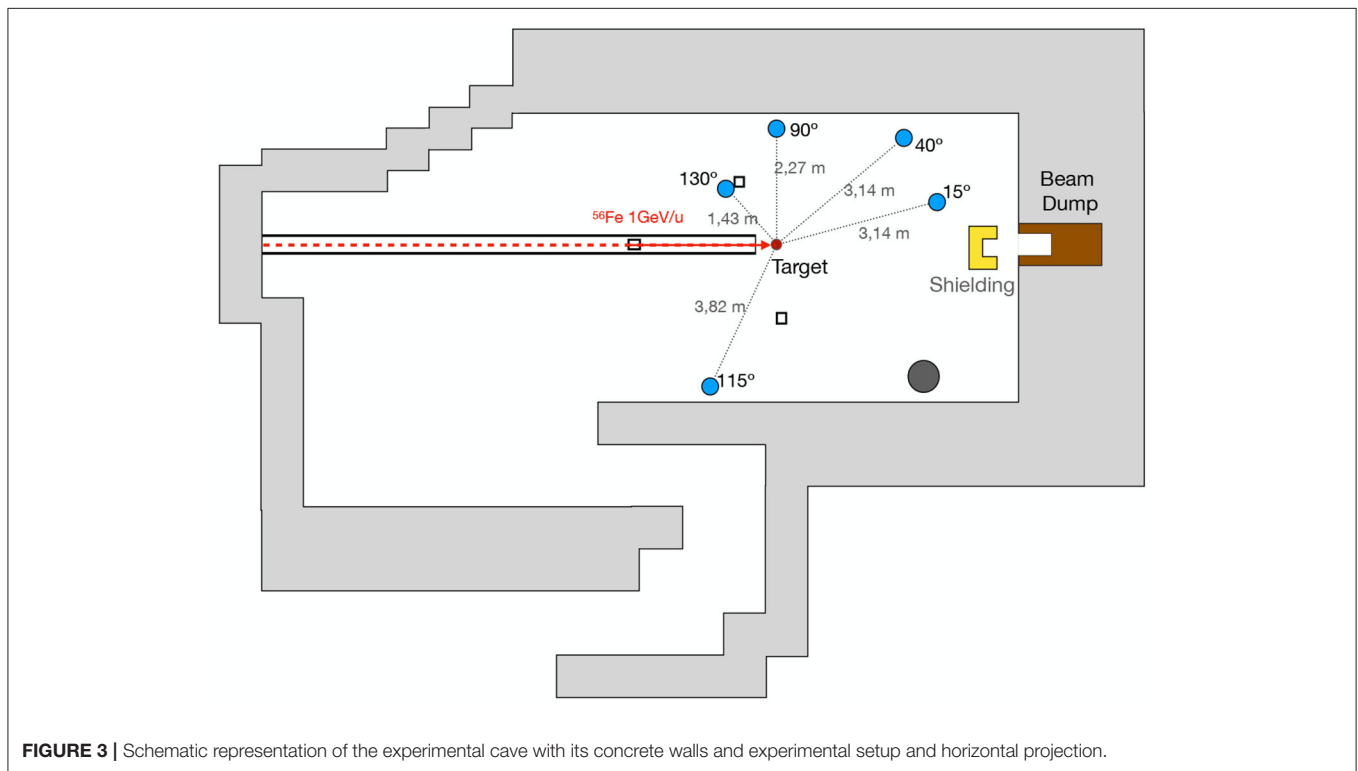


FIGURE 3 | Schematic representation of the experimental cave with its concrete walls and experimental setup and horizontal projection.

setup and of the experimental room is shown in **Figure 3**. The primary beam, a pencil beam (with a FWHM of about 1.2 cm), was constantly monitored during the irradiation with a parallel plate ionization chamber [35] while the beam position and focus was verified with Radiochromic films and a light screen. The beam monitor ionization chamber was calibrated in terms of primary particles by a dose measurement as described in detail in [36]. In order to reduce the contribution of back-scattered neutrons and of neutrons produced in the backwards direction—through the interaction of secondary radiation with the material present in the experimental room and with the walls—dedicated

PE shielding was placed in front of the beam dump and under the target position. The optimization of the shielding installation was performed with FLUKA simulations which allowed to define the most critical areas in the experimental room and establish reasonable measures to limit the background signal coming from the cave.

2.3. Cave Geometry and FLUKA Simulations

The FLUKA Monte Carlo particle transport code (version 2011.2x.5) [37, 38], used with the rQMD-2.4 model [39] and

in combination with the graphical user interface flair [40], has been used for the planning of the experiment and for the interpretation of the results. The whole setup, including the full Cave geometry, represented in **Figure 3** has been implemented in the simulation geometry and used to analyze the expected neutron and secondary particle field at the detector position and in the experimental area. All simulations have been performed with physics and transport parameters, including evaporation, coalescence, electromagnetic dissociation, and activation of the low-energy neutron optimized transport function. To compare with experimental values, the secondary neutron spectra have been scored in the detector volume, and the dosimeter response was then calculated by folding the simulated spectra with the energy-dependent response function of the GSI balls [41]. Additionally, the ambient dose equivalent calculated from ICRP74 [21] has been also scored in the volumes covered by the dosimeters.

Two-dimensional neutron ambient dose equivalent maps have been calculated in order to establish possible shielding approaches reducing the contribution of scattered neutrons at the measurement positions as much as possible. A 2D simulation of the dose equivalent distribution in the cave during the experiment is shown in **Figure 4** at the height of the beamline.

2.3.1. Secondary Proton Correction

As described in section 2.1, the subtraction of the TLD700H signal from the TLD600H signal allows the removal of contributions from particles other than neutrons. However, with this technique, enhancements of the TLD600H signal caused by tertiary neutrons produced within the GSI ball, for instance by secondary charged fragments, cannot be distinguished from real neutron dose. At small angles, close to the incident beam

direction, projectile fragments with high energies are present and might lead to a significant contribution especially for the 15° measurements. In particular, dose readings are expected to be perturbed by energetic protons that are able to reach the lead layer in the center of the GSI ball and produce spallation neutrons. The neutron ambient dose equivalents measured in the ^{56}Fe ion experiments described in this work were, thus, corrected for the contributions of secondary protons. The secondary proton spectra at the measurement positions were obtained from the FLUKA simulations of the experiment, see **Figure 5A**. However, as planned in the original IBER 17 project, secondary particle spectra were measured with ToF and energy loss measurements via ΔE -E telescopes. Those spectra were then used as the source in another FLUKA simulation where the GSI ball geometry is irradiated with protons, which is similar to the simulations performed to obtain the neutron response function of the dosimeter [41]. After normalizing the simulation results to the calibration field (^{241}Am -Be neutrons) and subtracting the TLD600H signal contributions induced directly by the incident protons (these doses are also measured by the TLD700H chips), the neutron dose readings obtained during the measurements can be corrected for the influence of secondary protons.

Projectile fragments heavier than protons (e.g. deuterons, tritons, or helium) were neglected in the correction of the dose readings since the perturbation due to those fragments can be considered as a second-order effect. Their fluences at the measurement positions were also scored

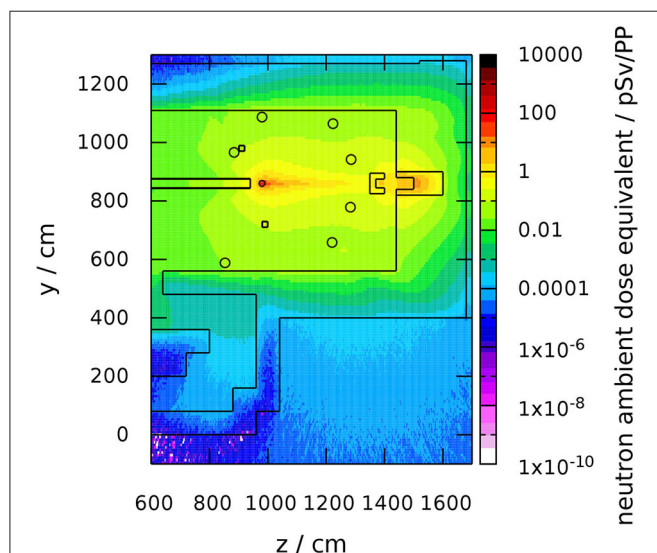


FIGURE 4 | Simulated neutron ambient dose equivalent distribution, normalized per primary particle, in the experimental room during the IBER 17 experiment.

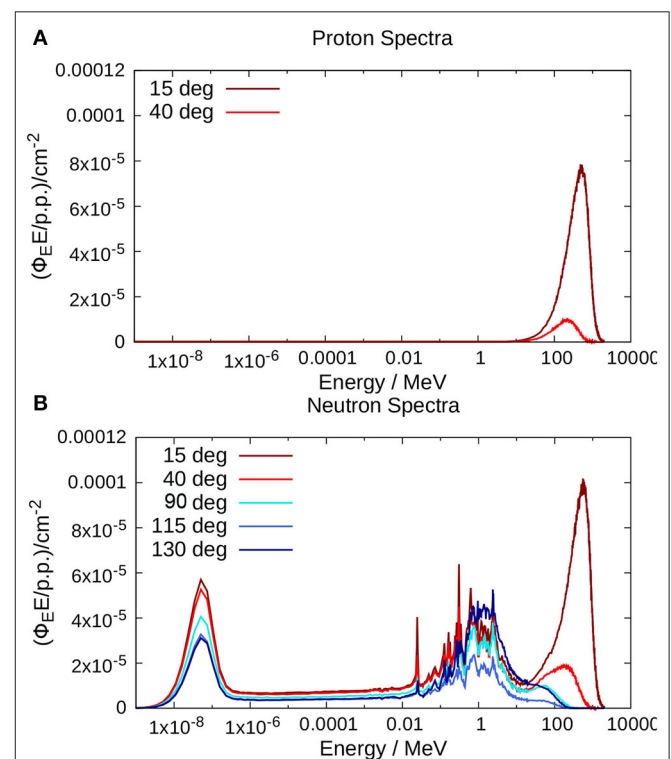


FIGURE 5 | (A) Calculated secondary proton spectrum at the 15 and 40 degree position. (B) Calculated neutron spectrum (fluence per unit lethargy) at the different dosimeter positions.

in the FLUKA simulation of the experiment but they were more than one order of magnitude smaller than the proton fluences.

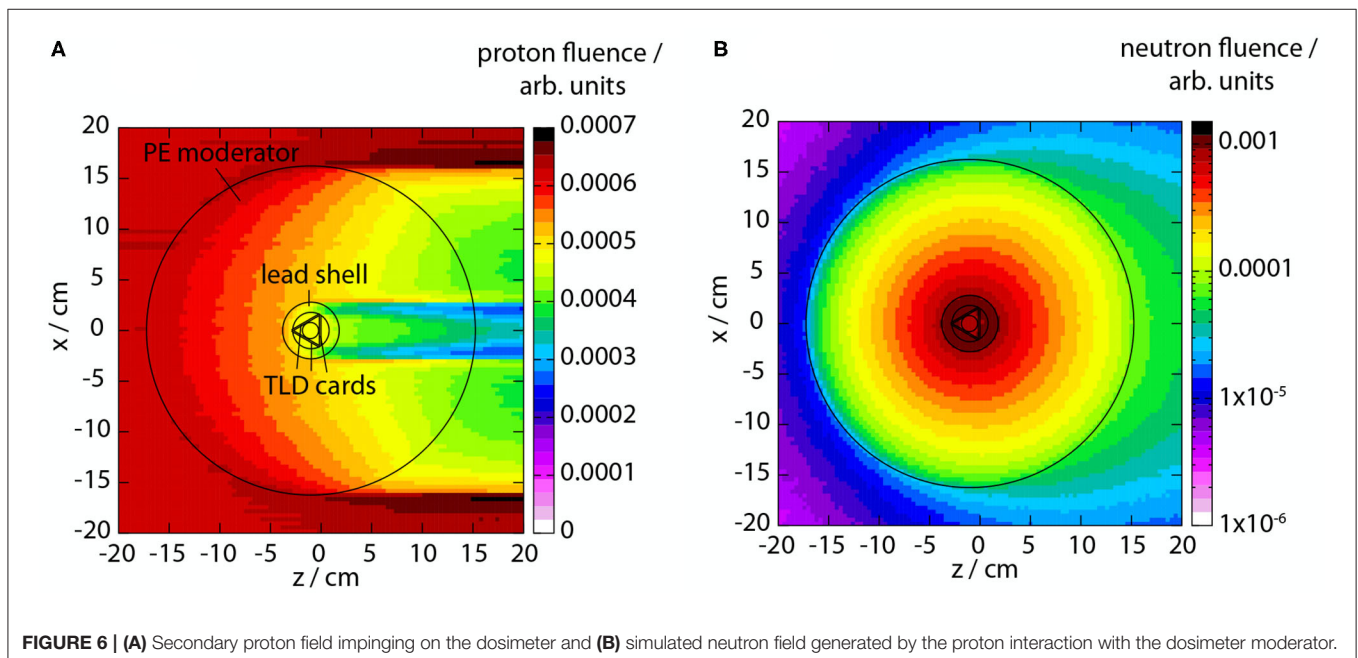
3. RESULTS AND DISCUSSION

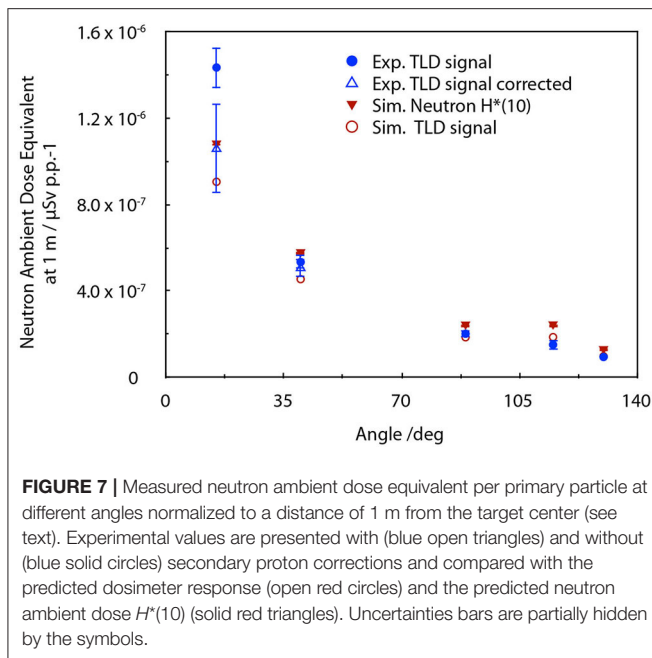
Results for the neutron ambient dose equivalent measured by the TLDs at the different positions normalized per primary particle are reported in **Table 1** together with the distances between the detector and the target center. For the two smallest angles, the contribution to the measured neutron dose equivalent coming from neutrons produced by the interaction of secondary protons with the moderator, and in particular with the lead layer included in the GSI ball, has been calculated with FLUKA simulations, and its effect on the measured values is also reported in **Table 1**. The simulated proton spectra in the detector volumes are shown in **Figure 5A** while **Figure 6** depicts 2D fluence maps of secondary protons and tertiary neutrons in the GSI ball. Despite the strong directionality of the secondary proton field, it can be observed that the generated neutron field at the TLD card position is

rather isotropic, thus justifying the use of an average correction on the reading of the three cards inside the detector. An effect of up to about 30% was found for the 15-degree position while a much lower contribution, of approximately 5%, is obtained at 40 degrees. A 30% uncertainty was estimated for the applied secondary proton corrections. Lower contributions are expected at larger angles justifying the application of the correction only at the two most forwarded angles. For kinematic reasons, indeed, the higher energy proton projectile fragments are produced in forward direction and are also visible from the simulated secondary proton spectra in **Figure 5A**. Experimental results have been compared to FLUKA predictions of the neutron ambient dose equivalent at the different measuring positions. A comparison of the calculated neutron ambient dose equivalent, $H^*(10)$ with the experimental measurements—with and without the neutron contribution coming from the secondary proton field—is shown in **Figure 7**. Even though the data analysis and simulation have been performed for the exact detector positions, for better visualization and interpretation, the data presented in **Figure 7** have been re-normalized to a 1 m distance

TABLE 1 | The neutron ambient dose equivalent per primary particle (p.p.) measured at the different dosimeter positions (reported distances are calculated from the center of the target center to the center of the dosimeters) are reported together with the measurement values corrected by the contribution of neutrons produced by the interaction of the secondary proton field with the dosimeter moderator (correction applied only to the two smallest angles).

Detector position/deg	Distance from the target center / m	Neutron ambient dose equivalent / $\mu\text{Sv/p.p.}$	Neutron ambient dose equivalent (with proton correction) / $\mu\text{Sv/p.p.}$
15	3.14	$1.5 \cdot 10^{-7} \pm 7\%$	$1.1 \cdot 10^{-7} \pm 20\%$
40	3.14	$5.4 \cdot 10^{-8} \pm 6\%$	$5.1 \cdot 10^{-8} \pm 8\%$
90	2.27	$3.9 \cdot 10^{-8} \pm 7\%$	$3.9 \cdot 10^{-8} \pm 7\%$
115	3.82	$1.0 \cdot 10^{-8} \pm 16\%$	$1.0 \cdot 10^{-8} \pm 16\%$
130	1.43	$4.6 \cdot 10^{-8} \pm 9\%$	$4.6 \cdot 10^{-8} \pm 9\%$





from the target center by applying the inverse square law. This normalization is only an approximation because it assumes idealized conditions with a point source and a constant neutron energy distribution at each angle scaling only with the distance from the target. However, it is useful to get an idea of the angular distribution of the neutron ambient dose equivalent because the distances between target and detectors were not equal for all measurement positions. For the experimental data, the uncertainty reported is the maximum between the statistical error on the detector reading and the standard deviation between the readings of the three cards held in a GSI ball. For the most forward angle, the calculated ambient dose equivalent is around 30% lower with respect to the measured value. However, after applying the correction for the secondary proton contribution this difference reduces significantly to a 2% difference. For large angles (40 to 130 degrees), the simulated neutron ambient dose equivalent results are always larger than the experimental values, showing an agreement within 25%. A larger deviation of about 40% is observed for the 115-degree angle. This significant difference is mainly due to larger uncertainties on the detector position introduced by the complexity of the Cave geometry and by the fact that this detector, different from the others, was not exactly at the beam height. These uncertainties can affect both the experimental results and the simulated contribution of scattered neutron from the walls and equipment present in the cave at the time of the experiment. Even though the detector readings are a good estimate for the neutron ambient dose equivalent, the expected detector response at the different measurement position has also been calculated by folding the simulated neutron spectra with the GSI ball response function. The simulated neutron spectra (fluence per unit lethargy) at the different dosimeter positions are shown in **Figure 5B**. For the small angles (forward direction with respect to the beam), the spectra are dominated

by a pronounced peak at about 560 MeV followed by two other smaller peaks: one at 1 MeV (evaporation neutrons) and one in the thermal neutron region. At larger angles, the high-energy peak becomes less important and disappears in the backward direction. This is because the higher-energy neutron projectile fragments show a pronounced forward direction due to the reaction kinematics while the evaporation neutrons are rather isotropic and the thermalized neutrons fill the cave homogeneously. The greater number of events reported in the 130 degree spectrum of this specific dosimeter was because it was positioned significantly closer to the target compared to the other detectors (only 1.43 m), see **Table 1** and **Figure 3**. The simulated detector responses, re-normalized to a 1 m distance from the target center, are also reported in **Figure 7**. At the larger angles, except for a deviation of 20% at 115 degrees, the measurements agree with the calculated detector response within 10%. However, at the 15 degree angle, an agreement of only 15% between the experimental data (including secondary fragment corrections) and the expected TLD response can be observed. Several factors might contribute to this deviation, including the contribution of additional neutrons generated by other secondary fragments here neglected and small inaccuracies in the geometry or material description in the FLUKA calculations (in a region where the neutron dose contribution has a large gradient).

For all investigated detector positions, the calculated $H^*(10)$ results always turned out to be larger than the measured and calculated GSI Ball responses. This can be explained because, in the neutron energy range between 0.1 and 500 MeV, the GSI ball response function underestimates the neutron ambient dose equivalent, see **Figure 1**.

4. CONCLUSION AND OUTLOOK

The work presented here is part of a larger experimental campaign aiming at the establishment of a multi-detector setup for the characterization of the neutron and light fragment field generated by galactic cosmic-ray-like radiation in thick shielding material. The mixed radiation field, generated by 1 GeV/u ^{56}Fe ions fully stopped in a thick aluminum target, has been characterized in terms of neutron ambient dose equivalent with GSI ball neutron dosimeters, the standard neutron dosimeter for area monitoring at the GSI accelerator facility. The neutron ambient dose has been measured at five different positions, and FLUKA calculations were carried out to predict the GSI ball response and the neutron ambient dose equivalent at the detector positions. Corrections at the more forward positions have been applied in order to exclude the contribution of tertiary (and higher-order) neutrons produced by the interaction of secondary protons with the detector moderator. The good agreement between the measured and calculated values—within a well-defined irradiation condition and using a standard reference ion beam and target material—demonstrated the validity of the approach and open up the possibility of investigating more complex irradiation scenarios. Different and less studied radiation qualities and more complex shielding materials could indeed be tested in future experiments with the presented

approach. Moreover, secondary fragment spectra measured with different experimental setups can be used for more accurate secondary proton and light fragment correction, as planned in future experiments. The capability of the GSI balls to give a good estimation of the neutron ambient dose equivalent over a range of neutron energies ranging from thermal to several GeVs makes these detectors particularly interesting for space radiation protection application. They allow us to get directly biologically relevant quantities also in complex radiation fields and for space relevant energies. They provide interesting data for benchmarking and validation of radiation transport codes and risk models. Additionally, thanks to the large range of energy covered, the possibility of measuring at very high intensities (being a passive detector it does not suffer from dead time effects) make this detector very suitable for ground based accelerator studies, especially for upcoming facilities like FAIR (Facility for Antiproton and Ion Research, Darmstadt, Germany) where ion beams of intensities up to 10^{11} particles/s (and protons up to 5×10^{12} particles/s) and energies up to 10 GeV/u (29 GeV for protons) will be reached.

DATA AVAILABILITY STATEMENT

The raw data supporting the conclusions of this article will be made available by the authors, without undue reservation.

REFERENCES

- Durante M, Cucinotta FA. Physical basis of radiation protection in space travel. *Rev Mod Phys.* (2011) **83**:1245–81. doi: 10.1103/RevModPhys.83.1245
- Cucinotta FA, Kim MHY, Chappell LJ. Report No.: NASA/TP-2011-216155. Space radiation cancer risk projections and uncertainties-2010 (2011).
- Durante M. Space radiation protection: destination Mars. *Life Sci Space Res.* (2014) **1**:2–9. doi: 10.1016/j.lssr.2014.01.002
- Norbury JW, Slaba TC, Aghara S, Badavi FF, Blattnig SR, Cloudsley MS, et al. Advances in space radiation physics and transport at NASA. *Life Sci Space Res.* (2019) **22**:98–124. doi: 10.1016/j.lssr.2019.07.003
- Walsh L, Schneider U, Fogtman A, Kausch C, McKenna-Lawlor S, Narici L, et al. Research plans in Europe for radiation health hazard assessment in exploratory space missions. *Life Sci Space Res.* (2019) **21**:73–82. doi: 10.1016/j.lssr.2019.04.002
- Norbury JW, Slaba TC. Space radiation accelerator experiments—the role of neutrons and light ions. *Life Sci Space Res.* (2014) **3**:90–4. doi: 10.1016/j.lssr.2014.09.006
- Walker SA, Townsend LW, Norbury JW. Heavy ion contributions to organ dose equivalent for the 1977 galactic cosmic ray spectrum. *Adv Space Res.* (2013) **51**:1792–9. doi: 10.1016/j.asr.2012.12.011
- Slaba TC, Blattnig SR, Norbury JW, Rusek A, La Tessa C. Reference field specification and preliminary beam selection strategy for accelerator-based GCR simulation. *Life Sci Space Res.* (2016) **8**:52–67. doi: 10.1016/j.lssr.2016.01.001
- Slaba TC, Bahadori AA, Reddell BD, Singleterry RC, Cloudsley MS, Blattnig SR. Optimal shielding thickness for galactic cosmic ray environments. *Life Sci Space Res.* (2017) **12**:1–15. doi: 10.1016/j.lssr.2016.12.003
- Nakamura T, Heilbronn L. *Handbook on Secondary Particle Production and Transport by High-Energy Heavy Ions.* World Scientific (2006). doi: 10.1142/5973

AUTHOR CONTRIBUTIONS

DB wrote the manuscript with support from FH. CS, MZ, EK, DR, CL, UW, MD, DB, and FH conceived and planned the experiments. DS, EK, DB, FH, CS, AS, ID, and MZ carried out the experiments. DS, EK, and DR, carried out the detector calibrations. DB and EK analyzed the data. DB and FH planned and carried out the simulations. TR and UW provided support and material for the experiment. All authors provided critical feedback and helped shape the manuscript.

FUNDING

This work was supported by European Space Agency (ESA)-IBER 17 project. The results are based on the experiment IBER-010, which was performed in Cave A at the GSI Helmholtzzentrum fuer Schwerionenforschung, Darmstadt (Germany) in the frame of FAIR Phase-0.

SUPPLEMENTARY MATERIAL

The Supplementary Material for this article can be found online at: <https://www.frontiersin.org/articles/10.3389/fphy.2020.00365/full#supplementary-material>

- Nakamura T, Heilbronn L. *Handbook on Secondary Particle Production and Transport by High-Energy Heavy Ions:(with CD-ROM).* World Scientific (2006).
- Castellanos, LA, McGirl NA, Srikrishna AP, Heilbronn L, La Tessa C, Rusek A, et al. “Thick-target yields of secondary ions and neutrons for validation of radiation transport codes,” in *2017 IEEE Aerospace Conference* (Big Sky, MT), 1–10. doi: 10.1109/AERO.2017.7943575
- Norbury JW, Miller J. Review of nuclear physics experimental data for space radiation. *Health Phys.* (2012) **103**:640–2. doi: 10.1097/HP.0b013e318261fb7f
- Norbury JW, Slaba TC, Sobolevsky N, Reddell B. Comparing HZETRN, SHIELD, FLUKA and GEANT transport codes. *Life Sci Space Res.* (2017) **14**:64–73. doi: 10.1016/j.lssr.2017.04.001
- Schuy C, Tessa CL, Horst F, Rovituso M, Durante M, Giraudo M, et al. Experimental assessment of lithium hydride’s space radiation shielding performance and Monte Carlo benchmarking. *Radiat Res.* (2019) **191**:154–61. doi: 10.1667/RR15123.1
- Rollet S, Agosteo S, Fehrenbacher G, Hranitzky C, Radon T, Wind M. Intercomparison of radiation protection devices in a high-energy stray neutron field, Part I: Monte Carlo simulations. *Radiat Meas.* (2009) **44**:649–59. doi: 10.1016/j.radmeas.2009.03.029
- Wiegel B, Agosteo S, Bedogni R, Caresana M, Esposito A, Fehrenbacher G, et al. Intercomparison of radiation protection devices in a high-energy stray neutron field, Part II: Bonner sphere spectrometry. *Radiat Meas.* (2009) **44**:660–72. doi: 10.1016/j.radmeas.2009.03.026
- Silari M, Agosteo S, Beck P, Bedogni R, Cale E, Caresana M, et al. Intercomparison of radiation protection devices in a high-energy stray neutron field. Part III: Instrument response. *Radiat Meas.* (2009) **44**:673–91. doi: 10.1016/j.radmeas.2009.05.005
- Fehrenbacher G, Gutermuth F, Kozlova E, Radon T, Schuetz R. Neutron dose measurements with the GSI ball at high-energy accelerators. *Radiat Protect Dosimet.* (2007) **125**:209–12. doi: 10.1093/rpd/ncl127

20. Gutermuth F, Radon T, Fehrenbacher G, Festag J. The response of various neutron dose meters considering the application at a high energy particle accelerator. *Kerntechnik*. (1987). **68**:172–9.
21. ICRP. *Conversion Coefficients for Use in Radiological Protection Against External Radiation*. ICRP Publication 74 Ann ICRP (1996). doi: 10.1016/S0146-6453(96)90003-2
22. Fehrenbacher G, Kozlova E, Gutermuth F, Radon T, Schütz R, Nolte R, et al. Measurement of the fluence response of the GSI neutron ball dosimeter in the energy range from thermal to 19 MeV. *Radiat Protect Dosimet.* (2007) **126**:546–8. doi: 10.1093/rpd/ncm110
23. Fehrenbacher G, Gutermuth F, Kozlova E, Radon T, Aumann T, Beceiro S, et al. Measurement of the fluence response of the GSI neutron ball in high-energy neutron fields produced by 500 AMeV and 800 AMeV deuterons. *Radiat Protect Dosimet.* (2007) **126**:497–500. doi: 10.1093/rpd/ncm100
24. Sannikov A, Savitskaya E. Ambient dose equivalent conversion factors for high energy neutrons based on the ICRP 60 recommendations. *Radiat Protect Dosimet.* (1997) **70**:383–6. doi: 10.1093/oxfordjournals.rpd.a031982
25. Pelliccioni M. Overview of fluence-to-effective dose and fluence-to-ambient dose equivalent conversion coefficients for high energy radiation calculated using the FLUKA code. *Radiat Protect Dosimet.* (2000) **88**:279–97. doi: 10.1093/oxfordjournals.rpd.a033046
26. Lee J, Pradhan A, Kim J, Kim B, Yim K. Response of 6LiF: Mg, Cu, Si and 7LiF: Mg, Cu, Si TLD pairs to the neutrons and photon mixtures. *J Nuclear Sci Technol.* (2008) **45**:233–6. doi: 10.1080/00223131.2008.10875830
27. Vega-Carrillo HR. TLD pairs, as thermal neutron detectors in neutron multisphere spectrometry. *Radiat Meas.* (2002) **35**:251–4. doi: 10.1016/S1350-4487(01)00291-8
28. Vega-Carrillo HR, Guzman-Garcia KA, Gallego E, Lorente A. Passive neutron area monitor with pairs of TLDs as neutron detector. *Radiat Meas.* (2014) **69**:30–4. doi: 10.1016/j.radmeas.2014.08.006
29. *Thermo Scientific Harshaw TLD Materials and Dosimeters*. Technical report. BRRMSI-TLD-0616 (2016). Available online at: <https://assets.thermofisher.com/TFS-Assets/LSG/Catalogs/Dosimetry-Materials-Brochure.pdf>
30. Kozlova E, Sokolov A, Pyshkina M, Radon T. *Testing of New Sensitive TLD Cards*. GSI Scientific Report (2016).
31. RadPro Product Brochure. *RadPro International GmbH*. (2020). Available online at: <https://www.radpro-int.com>
32. Horowitz Y, Olko P. The effects of ionisation density on the thermoluminescence response (efficiency) of LiF:Mg,Ti and LiF:Mg,Cu,P. *Radiat Protect Dosimet.* (2004) **109**:331–48. doi: 10.1093/rpd/nch310
33. Eisenhauer C. Two-component analytical model to calculate room-return correction for calibration of neutron instruments. *Radiat Protect Dosimet.* (1992) **42**:267–77.
34. Vega-Carrillo HR, Manzanares-Acu na E, I niguez MP, Gallego E, Lorente A. Study of room-return neutrons. *Radiat Meas.* (2007) **42**:413–9. doi: 10.1016/j.radmeas.2007.01.036
35. Kraft G, Weber U. Tumor therapy with ion beams. In: *Handbook of Particle Detection and Imaging*. Berlin; Heidelberg: Springer-Verlag (2012). p. 1179. doi: 10.1007/978-3-642-13271-1_47
36. Luoni F, Weber U, Boscolo D, Reidel CA, Zink K, Horst F. Beam monitor calibration for radiobiological experiments with scanned high energy heavy ion beams for FAIR. *Front Phys.* (2020) **8**:568145. doi: 10.3389/fphy.2020.568145
37. Battistoni G, Boehlen T, Cerutti F, Chin PW, Esposito LS, Fassó A, et al. Overview of the FLUKA code. *Ann Nuclear Ener.* (2015) **82**:10–8. doi: 10.1016/j.anucene.2014.11.007
38. Fassó A, Ferrari A, Ranft J, Sala PR. Report No.: CERN-2005-010, SLAC-R-773, INFN-TC-05-11. *FLUKA: A Multi-Particle Transport Code*. CERN Yellow Reports: Monographs (2005). doi: 10.2172/877507
39. Sorge H, Stöcker H, Greiner W. Poincaré invariant Hamiltonian dynamics: modelling multi-hadronic interactions in a phase space approach. *Ann Phys.* (1989) **192**:266–306. doi: 10.1016/0003-4916(89)90136-X
40. Vlachoudis V. FLAIR: a powerful but user friendly graphical interface for FLUKA. In: *Proc. Int. Conf. on Mathematics, Computational Methods & Reactor Physics (M&C 2009)*. Saratoga Springs, NY (2009).
41. Horst F, Fehrenbacher G, Zink K. On the neutron radiation field and air activation around a medical electron linac. *Radiat Protect Dosimet.* (2017) **174**:147–58. doi: 10.1093/rpd/ncw120

Conflict of Interest: The authors declare that the research was conducted in the absence of any commercial or financial relationships that could be construed as a potential conflict of interest.

Copyright © 2020 Boscolo, Scognamiglio, Horst, Weber, Schuy, Durante, La Tessa, Kozlova, Sokolov, Dinescu, Radon, Radeck and Zbořil. This is an open-access article distributed under the terms of the Creative Commons Attribution License (CC BY). The use, distribution or reproduction in other forums is permitted, provided the original author(s) and the copyright owner(s) are credited and that the original publication in this journal is cited, in accordance with accepted academic practice. No use, distribution or reproduction is permitted which does not comply with these terms.